

# Momentum-resolved time evolution with matrix product states

Maarten Van Damme\* and Laurens Vanderstraeten†

*Department of Physics and Astronomy, University of Ghent, Krijgslaan 281, 9000 Gent, Belgium*

We introduce a new method based on matrix product states (MPS) for computing spectral functions of (quasi) one-dimensional spin chains, working directly in momentum space in the thermodynamic limit. We simulate the time evolution after applying a momentum operator to an MPS ground state by working with the momentum superposition of a window MPS. We show explicitly for the spin-1 Heisenberg chain that the growth of entanglement is smaller in momentum space, even inside a two-particle continuum, such that we can attain very accurate spectral functions with relatively small bond dimension. We apply our method to compute spectral lineshapes of the gapless XXZ chain and the square-lattice  $J_1$ - $J_2$  Heisenberg model on a six-leg cylinder.

**Introduction**— Spectral functions are one of the most important tools for relating theory and experiment in the field of strongly-correlated quantum matter. Indeed, the most exotic properties of strongly-correlated quantum phases are typically related to the low-energy excitations in these systems, for which the spectral function is a direct experimental probe. Here, inelastic neutron scattering for magnetic materials and angle-resolved photoemission spectroscopy for electronic systems serve as the most common options. For example, in the last years the occurrence of fractionalized quasiparticles in candidate two-dimensional spin-liquid materials can be observed through the spectral function in neutron-scattering experiments [1, 2].

A pressing challenge on the theoretical side is the evaluation of the spectral function for a given microscopic model Hamiltonian. In the one-dimensional case, a restricted class of integrable models such as the spin-1/2 Heisenberg chain [3] allows for a quasi-exact computation of the spectral function. In two dimensions, besides the case of the Kitaev spin liquid [4, 5], exact calculations are even less common. Traditional numerical methods include exact diagonalization with a continued fraction expansion [6], which is limited to small clusters, and quantum Monte Carlo, for which the analytic continuation [7–9] to real frequencies is often uncontrolled. Variational methods for capturing excited states based on Gutzwiller-projected mean-field states [10, 11] or, more recently, variational wavefunctions from machine learning [12].

For one-dimensional lattice systems, a lot of effort went into designing efficient numerical methods based on the formalism of matrix product states (MPS) [13]. The earliest approaches were based on the continued-fraction expansion [14, 15] or correction vectors [16–18]; the latter can give very accurate results, but requires a different run for every frequency and requires adding a small imaginary frequency leading to significant broadening. Using Chebyshev expansions for the spectral function, the full frequency range can be computed in a single run [19–

21]. Alternatively, one can use time-dependent MPS algorithms [22–26] for computing the real-time evolution after applying a local operator to the ground state, and transform to frequency space [27]; here, the frequency resolution is limited due to the growth of entanglement in the time-evolved state, although linear prediction [27–29] or recursion methods can be used to extrapolate the signal to longer times [30].

Although the spectral function is a momentum-resolved quantity, in all these MPS approaches the translation symmetry of the model is explicitly broken either by working on a finite open-boundary system or by introducing a local operator for time evolution. A viable alternative consists of targeting the low-energy excitations by a variational “quasiparticle ansatz” that has well-defined momentum directly in the thermodynamic limit [31, 32]. With this approach, one can compute the dispersion and spectral weight of isolated branches in the spectrum [33] with high precision [34, 35]; this method does not suffer from a finite resolution in momentum and frequency, but only from variational errors. Extending this framework to two-particle excitations [36, 37], the fine-grained features of the spectral function within a two-particle continuum can be resolved [38]. For critical systems however, the absence of isolated lines or the occurrence of multi-particle continua make this variational approach less useful for obtaining the full spectral function accurately.

In this paper, we introduce an MPS-based method for simulating time evolution directly in momentum space and the thermodynamic limit, which enables us to compute spectral functions with higher accuracy than a real-space approach would with the same bond dimension. We first recapitulate how the real-space approach works using a window MPS embedded in a uniform background, and then discuss how to lift this approach to momentum space. We illustrate our method by comparing the real and momentum-space approaches for the spectral function in the two-magnon continuum in the spin-1 Heisenberg chain. We further illustrate the efficiency of our momentum-resolved method by simulating the time evolution of wavepackets, thus interpolating between real and momentum space. Finally, we benchmark our method by computing spectral lineshapes for the gap-

\* Maarten.VanDamme@ugent.be

† Laurens.Vanderstraeten@ugent.be

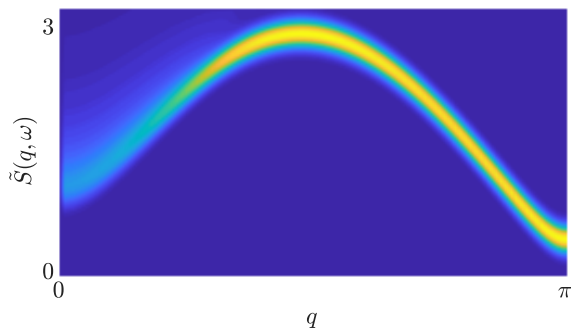


FIG. 1. **Spectral function for spin-1 chain.** We have rescaled the spectral function with the integrated spectral weight, i.e. we plot  $\tilde{S}(q, \omega) = S(q, \omega) / \int d\omega S(q, \omega)$ . Here we have used SU(2) invariant MPS with total bond dimension  $D \approx 1000$ , a real-space window of  $N_w = 201$ , evolved with a cluster-expansion MPO up to times  $T = 30$ , and applied a window function with  $\alpha = 5$ .

less XXZ chain and the square-lattice  $J_1$ - $J_2$  Heisenberg model on a six-leg cylinder.

**Real-space approach**— Let us consider the spin-1 Heisenberg chain with Hamiltonian

$$H = \sum_{\langle ij \rangle} \vec{S}_i \cdot \vec{S}_j, \quad \vec{S}_i = (S_i^x, S_i^y, S_i^z), \quad (1)$$

where  $S_i^\alpha$  are the spin-1 operators at site  $i$  and the sum runs over all nearest neighbours. Here we are interested in the momentum-frequency resolved spectral function at zero temperature

$$S(q, \omega) = \int_{-\infty}^{\infty} dt e^{i\omega t} S(q, t), \quad (2)$$

with

$$S(q, t) = \sum_{n'} e^{-iqn'} \sum_{\alpha} \langle \Psi_0 | S_{n+n'}^{\alpha} e^{-i(H-E_0)t} S_n^{\alpha} | \Psi_0 \rangle, \quad (3)$$

and  $|\Psi_0\rangle$  the ground state with ground-state energy  $E_0$ ; site  $n$  is an arbitrary location in the translation-invariant system.

First we can approximate the ground state directly in the thermodynamic limit with a uniform MPS described by a single tensor  $A$

$$|\Psi_0\rangle = \cdots - \boxed{A} - \boxed{A} - \boxed{A} - \boxed{A} - \boxed{A} - \cdots \quad (4)$$

Starting from the ground state, we can apply a single-site spin operator at an arbitrary site  $n$  and time-evolve the state,

$$|\Psi_n^{\alpha}(t)\rangle_{\text{rs}} = e^{-i(H-E_0)t} S_n^{\alpha} |\Psi_0\rangle. \quad (5)$$

The perturbation induced by the operator is expected to spread through the system as time evolves, such that this

time-evolved state should be approximated as an MPS with a window of site-dependent tensors around site  $n$ , embedded within the uniform MPS [39–41]

$$|\Psi_n^{\alpha}(X)\rangle_{\text{rs}} \approx \cdots - \boxed{A} - \boxed{X_1} - \cdots - \boxed{X_N} - \boxed{A} - \cdots \quad (6)$$

In this ansatz, the bond dimension of the tensors  $X_i$  and the size of the window  $N_w$  enter as control parameters, and both are expected to grow as time evolves: the effect of applying a local operator will spread through the system with a characteristic velocity and the entanglement due to the spread of quasiparticles will grow.

The time evolution of the tensors  $X_i$  can be determined via the time-dependent variational principle (TDVP) [24, 42] or by applying the time-evolution operator and truncating the bond dimension [26]. Here we take the latter option, i.e. in each time step we want to find new tensors  $X'_i$  such that

$$|\Psi_n(X')\rangle_{\text{rs}} \approx e^{-i(H-E_0)\delta t} |\Psi_n(X)\rangle_{\text{rs}} \quad (7)$$

for a time step  $\delta t$ . This equation can be interpreted variationally such that we find tensors  $X'_i$  that maximize the overlap with the right-hand side, which in practice is achieved by a sweeping algorithm that sequentially optimizes over the different tensors; here, exploiting the canonical form and changing the orthogonality center within the window is crucial for a stable algorithm [13].

A crucial ingredient in this approach is finding an efficient matrix product operator representation of the time-evolution operator  $e^{-i(H-E_0)\delta t}$ , where ideally we would like to large time steps  $\delta t$ . For local interactions a Trotter-Suzuki decomposition [43–45] has been the most straightforward option, but recently a cluster expansion was introduced that allows us to take rather large time steps  $\delta t$  with a modest bond dimension and high accuracy [46, 47]. For long-range interactions, a simple prescription allows us to approximate the time-evolution operator up to first order; the result is known as the  $W_1$  operator, which can be extended to also include some higher-order terms with the same bond dimension [25]. In the Appendix of this work [App. B], we show that we can systematically extend this construction to higher orders.

Note that we can split up the full time evolution into

$$S(q, t + t') = \sum_{n'} e^{-iqn'} \sum_{\alpha} \langle \Psi_{n+n'}^{\alpha}(-t') | \Psi_n^{\alpha}(t) \rangle_{\text{rs}}, \quad (8)$$

where bra and ket states can be time-evolved independently; this allows to reach longer times for  $S(q, t)$  accurately with a given bond dimension in both time-evolved states. Finally, in the following we always apply a Gaussian window function to the finite-time signal when transforming to the frequency plane,

$$S(q, \omega) \sim \int_0^T dt e^{i\omega t} e^{-\alpha \frac{t^2}{T^2}} \left( S(q, t) + \overline{S(q, t)} \right), \quad (9)$$

in order to avoid unphysical signatures of the finite-time simulation in the spectral function. As mentioned above,

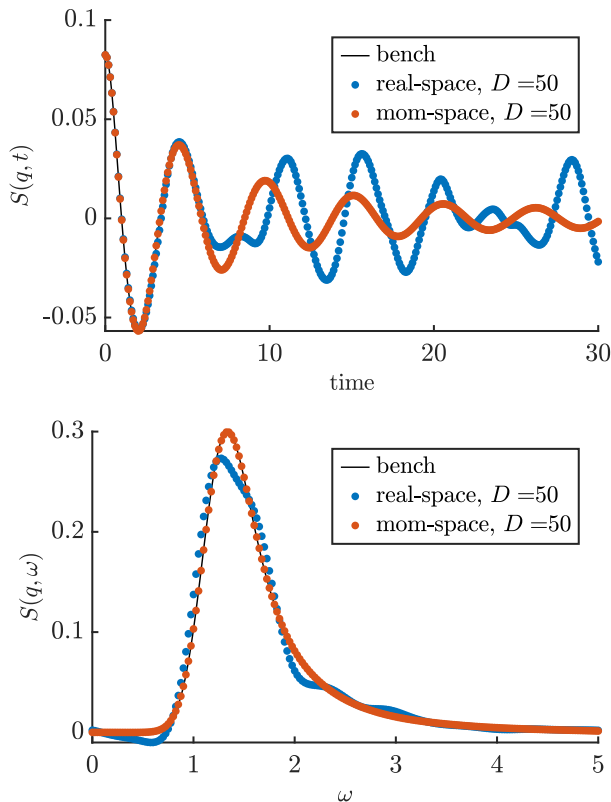


FIG. 2. **Comparing the accuracy of real-space and momentum-space approaches.** We plot the real-time signal  $S(q, t)$  and the resulting spectral function  $S(\omega, t)$  for the momentum cut  $q = \pi/10$  inside the two-magnon continuum. We have used SU(2)-symmetric MPS with total bond dimension  $D = 50$ , and one-sided time evolution for the sake of comparison. The benchmark result was run at a bond dimension  $D \approx 1500$ .

extrapolation techniques can be used for extending the time signal [27–30], but in this paper we refrain from exploiting this to focus on the accuracy of the time-evolution method itself.

Using this approach, in Fig. 1 we have plotted the spectral function for the spin-1 Heisenberg chain in the full Brillouin zone. We can identify an isolated magnon mode around momentum  $q = \pi$  and a more diffuse two-magnon continuum around momentum  $q = 0$  [27]. The integrated spectral weight goes to zero as  $q \rightarrow 0$ , so in order to clearly show these two regimes we have rescaled each momentum cut such that the integrated weight is constant throughout the Brillouin zone.

**Momentum-space evolution**— Let us now explain how to evaluate the spectral function directly in momentum space. Here, we start from rewriting the spectral function as an overlap between two states with well-defined momentum

$$S(q, t) = \langle \Psi_q(0) | \Psi_q(t) \rangle_{\text{finite}}, \quad (10)$$

with

$$|\Psi_q^\alpha(t)\rangle = e^{-i(H-E_0)t} \sum_n e^{iqn} S_n^\alpha |\Psi_0\rangle, \quad (11)$$

and where we have defined the finite part of the overlap between two momentum states as

$$\langle \Psi_p | \Psi_q \rangle = 2\pi\delta(p - q) \langle \Psi_p | \Psi_q \rangle_{\text{finite}}. \quad (12)$$

The central idea in this work is to represent this time-evolved momentum state as a “momentum-window MPS” [48] of the form

$$|\Psi_q^\alpha(t)\rangle_{\text{ms}} \approx \sum_n e^{iqn} \left( \dots - \boxed{A} - \boxed{X}_n - \dots - \boxed{X}_N - \boxed{A} - \dots \right). \quad (13)$$

Similarly as for the real-space window, the size of the window  $N_w$  and the bond dimension of the tensors  $X_i$  enter as control parameters.

For a momentum cut that is dominated by a single mode (e.g., the magnon in Fig. 1), we know that this momentum-window MPS will capture the time evolution very well. Indeed, the variational quasiparticle ansatz is contained within the class of momentum-window states, so in all cases for which the former yields high-precision eigenstates (i.e., isolated lines in the spectrum [33]) we will be able to simulate long time evolution accurately with a momentum-window state. For two-particle states, we have captured the “center-of-mass” motion by going to momentum space, whereas the relative motion between the two particles will have to be accounted for by growing the size of the momentum window.

Besides smaller windows, we expect that the bond dimension within the window will grow less rapidly than in the real-space approach. Indeed, since the translation symmetry of the model is explicitly preserved throughout the calculations, we can target one specific momentum sector only. This means that the time-evolved momentum window contains a lot less information, and can therefore be represented with a smaller bond dimension.

The downside of the momentum-space approach is that a time-evolution algorithm is more complex, but we can apply a few tricks to make it more efficient. Clearly, the initial state at  $t = 0$  can be written exactly as such a momentum-window MPS without much effort. As we show in the Appendix, the gauge conditions on the ground-state MPS tensors allow us to fix the first tensor  $X_1$  such that the overlap between two momentum-window MPSs reduces to the inner product of the window tensors only. Additionally, we can exploit the canonical form for the window MPS to shift the orthogonality center around within the window, which makes it possible to use standard finite-MPS sweeping algorithms and local updates for optimizing the tensors in each time step. Due to the momentum superposition, however, the effective operators that appear in the local updates of the tensors consist of a number of terms scaling linearly with

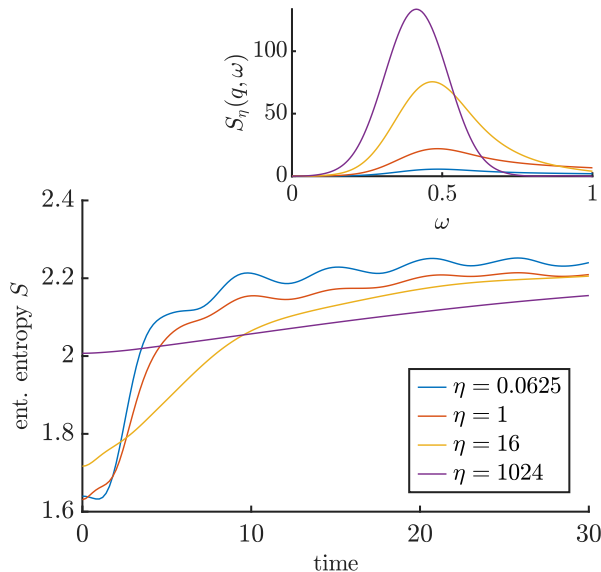


FIG. 3. **Interpolating between real space and momentum space.** The main panel shows the bipartite entanglement entropy as a function of time, measured for a cut next to the center of the wavepacket. In the inset, we show the convoluted spectral functions. These simulations were done at  $D = 320$  with a real-space window MPS of size  $N_w = 257$ ,  $T = 30$  and  $\alpha = 5$ .

the window size  $N_w$ ; this should be compared by just a single term in the real-space approach. The good news is that these terms can all be computed in parallel, such that with enough parallel workers the run time should be comparable. Again, we can either use the TDVP or apply the time-evolution operator variationally; as we show in the Appendix, the latter appears to be simpler and more efficient for evolving momentum-window MPS.

We can illustrate the efficiency of the momentum-window state by applying it to the spin-1 chain. We find that we can simulate the real-time correlator  $S(q, t)$  at momentum  $q = \pi$  with high precision up to arbitrary large times with moderate bond dimension (not shown), which follows directly from the fact that the quasiparticle ansatz yields quasi-exact results for the magnon mode [24]. The two-magnon continuum is potentially more challenging: In Fig. 2 we show the results for a momentum cut in the two-particle region  $q = \pi/10$ , where we compare the time correlator as evaluated with a real-space and momentum-space window. We have taken sufficiently large window sizes and the same bond dimension, showing clearly that the real-space approach becomes inaccurate rather quickly whereas the momentum-space approach is still accurate at long times. In the spectral function  $S(q, \omega)$  the difference is equally clear.

**Interpolating between spaces**— In order to explicitly show that momentum states develop less entanglement than real-space states, we will interpolate between these two limits by considering wavepacket states. Indeed, we

will consider a convoluted spectral function

$$S^\eta(q, t) = \sqrt{4\pi\eta} \int \frac{dq'}{2\pi} e^{-\eta(q-q')^2} S(q', t), \quad (14)$$

such that  $\lim_{\eta \rightarrow \infty} S^\eta(q, t) = S(q, t)$ . We can write this as the overlap between wavepacket states of the form

$$|\Psi_q^\eta(t)\rangle = e^{-i(H-E_0)t} \sum_n \int \frac{dq'}{2\pi} e^{-\frac{\eta}{2}(q-q')^2 + iq'n} S_n, \quad (15)$$

as

$$S^\eta(q, t) = \langle \Psi_q^\eta(0) | \Psi_q^\eta(t) \rangle. \quad (16)$$

We can now prepare these states centered around a given site in the lattice and time evolve the state using the real-space window MPS. In the inset of Fig. 3 we have plotted the convoluted spectral function around momentum  $q = \pi$ , for which the magnon mode reaches its minimal energy. For very large  $\eta$  we observe the magnon mode (smeared out due to the window function), and by decreasing  $\eta$  the spectral weight partially shifts to other momenta and, therefore, to larger frequencies. Crucially, the main panel shows that (i) the initial entanglement of a real-space localized wavepacket is smaller, but (ii) the increase of entanglement through time is a lot larger. The larger initial entanglement occurs because we are representing a momentum superposition in real space, but this zero-time offset can be transformed away by performing all calculations in momentum space directly. This result, therefore, confirms that a momentum-resolved time evolution will require a smaller bond dimension for the same accuracy.

**Benchmarks**— Let us now perform some benchmarks on more challenging models. First we take the spin-1/2 XXZ chain, defined by the Hamiltonian

$$H_{\text{XXZ}} = \sum_{\langle ij \rangle} S_i^x S_j^x + S_i^y S_j^y + \Delta S_i^z S_j^z, \quad (17)$$

where  $S_i^\alpha$  are now spin-1/2 operators. We take  $\Delta = 1/2$  in the gapless phase, and investigate a cut of the spectral function at momentum  $q = \pi/2$ . It is known from Luttinger-liquid theory [49] that the spectral function diverges at the edge of the continuum, which has been confirmed by MPS methods [28]. Moreover, the continuum consists of multi-spinon states and therefore is a good check for our method. In Fig. 4 we show a comparison between the real-space and momentum-space approaches, again showing that the latter is more precise for the same bond dimension. In particular, the inset shows that the momentum-space window can capture the exact time evolution for significantly longer times.

Finally, we consider the  $J_1$ - $J_2$  Heisenberg model on the square lattice,

$$H = J_1 \sum_{\langle ij \rangle} \vec{S}_i \cdot \vec{S}_j + J_2 \sum_{\langle\langle ij \rangle\rangle} \vec{S}_i \cdot \vec{S}_j. \quad (18)$$

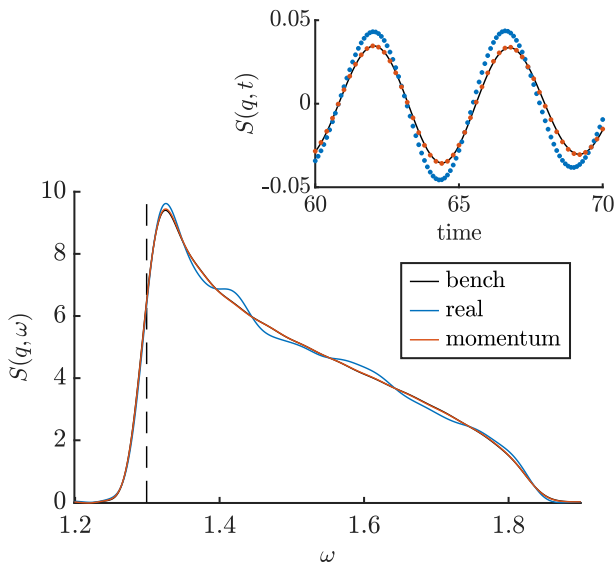


FIG. 4. **Spectral function for the XXZ chain.** We compare a real-space and momentum-space computation for  $S(q, \omega)$  at the same bond dimension  $D \approx 100$ , with a window size of  $N_w = 257$  and  $N_w = 64$  for the real-space and momentum-space window, resp. We have evolved for a total time of  $T = 128$  and used a window function with  $\alpha = 3$ . The vertical line is the edge of the continuum known exactly from the Bethe ansatz. The inset shows a portion of the real-time signals. We compare to a benchmark simulation with bond dimension  $D = 1568$ . We have used  $U(1)$  symmetry and a two-site uniform MPS in these simulations.

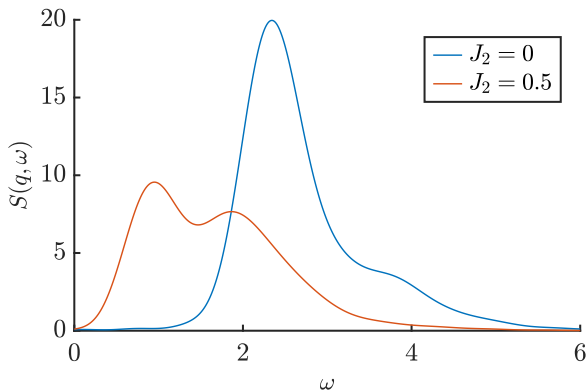


FIG. 5. **Spectral function for the  $J_1$ - $J_2$  model for momentum  $q = (\pi, 0)$  on a six-leg cylinder.** We have evolved until total time  $T = 9.5$  and applied a window function with  $\alpha = 4$ ; in both cases we have used  $SU(2)$  symmetry, a bond dimension around  $D \approx 400$  and a window size of  $N_w = 24$ .

Determining the phase diagram of the full two-dimensional model has been the subject of many numerical works, and getting accurate and unbiased results for the spectral function is important for getting an insight into the fractionalized spinon excitations in the putative spin-liquid phase. Even for the nearest-neighbour case ( $J_2 = 0$ ) there is the occurrence of a dip in the magnon

dispersion relation at momentum  $(\pi, 0)$  [50] for which many physical mechanisms have been proposed [9, 51–53]. This dip is expected to further drop in energy, until it becomes gapless in the spin-liquid phase [52, 54].

Here we simulate the model on a six-leg cylinder and use our momentum-space approach to compute a cut of the spectral function for momentum  $q = (\pi, 0)$  for the unfrustrated case ( $J_2 = 0$ ) and for  $J_2/J_1 = 0.5$ ; in Fig. 5 the results are presented. For  $J_2 = 0$  we find a gap that is in agreement with other methods [9, 51–53, 55]. We clearly see that the gap has decreased significantly in the frustrated case, and that the spectrum is less peaked and more diffuse, which is suggestive of a fractionalized multi-spinon continuum. Nonetheless, we find that the gap is still quite large and we observe a two-peak structure in the lineshape. We have computed the gap using the quasiparticle ansatz for cylinders [35] and obtained a similar value (not shown), suggesting that this is a genuine feature of the six-leg cylinder.

**Conclusions**— In this paper we have introduced a new MPS-based method for calculating spectral functions, relying on an efficient scheme for time-evolving momentum states. We have benchmarked our method against the traditional real-space approach and obtain accurate results at relatively low bond dimensions. We expect that our method will be very useful in combination with a real-space approach: the latter allows us to find the full spectral function in a single run, whereas the former can be used for resolving fine-grained structures in certain momentum cuts. In particular, this strategy can be useful for tackling quasi two-dimensional systems with strong correlations such as spin liquids and Hubbard models, for which MPS simulations are currently limited [51, 56–59].

In our work we have solely relied on time evolution for computing spectral functions, but we can also explore the momentum-space version of other strategies such as the correction-vector method. Note that previous works have indeed used momentum states on finite systems [15, 16, 19, 21, 60], but without exploiting the structure of the momentum superposition directly in the thermodynamic limit.

The ability to obtain high precision results at lower bond dimensions is of primary importance when applying projected entangled-pair states (PEPS), the two-dimensional version of MPS, where computational complexity scales unfavourably in bond dimension. Following the success of existing tangent-space methods for PEPS [55, 61, 62], we should be able to generalize our momentum-resolved scheme to higher spatial dimensions, and enable the calculation of high-precision spectral functions with PEPS.

**Acknowledgments**— We acknowledge inspiring discussion with Markus Drescher, Jutho Haegeman, Wilhelm Kadow, Michael Knap, Frank Pollmann, Frank Verstraete, and Elisabeth Wybo. This work was supported by the Research Foundation Flanders.

- 
- [1] T.-H. Han, J. S. Helton, S. Chu, D. G. Nocera, J. A. Rodriguez-Rivera, C. Broholm, and Y. S. Lee, Fractionalized excitations in the spin-liquid state of a kagome-lattice antiferromagnet, *Nature* **492**, 406 (2012).
- [2] A. Banerjee, C. Bridges, J.-Q. Yan, A. Aczel, L. Li, M. Stone, G. Granroth, M. Lumsden, Y. Yiu, J. Knolle, *et al.*, Proximate kitaev quantum spin liquid behaviour in a honeycomb magnet, *Nature materials* **15**, 733 (2016).
- [3] M. Mourigal, M. Enderle, A. Klöpperpieper, J.-S. Caux, A. Stunault, and H. M. Rønnow, Fractional spinon excitations in the quantum heisenberg antiferromagnetic chain, *Nature Physics* **9**, 435 (2013).
- [4] J. Knolle, D. L. Kovrizhin, J. T. Chalker, and R. Moessner, Dynamics of a two-dimensional quantum spin liquid: Signatures of emergent majorana fermions and fluxes, *Phys. Rev. Lett.* **112**, 207203 (2014).
- [5] J. Knolle, D. L. Kovrizhin, J. T. Chalker, and R. Moessner, Dynamics of fractionalization in quantum spin liquids, *Phys. Rev. B* **92**, 115127 (2015).
- [6] E. R. Gagliano and C. A. Balseiro, Dynamical properties of quantum many-body systems at zero temperature, *Phys. Rev. Lett.* **59**, 2999 (1987).
- [7] H. B. Schüttler and D. J. Scalapino, Monte carlo studies of the dynamical response of quantum many-body systems, *Phys. Rev. B* **34**, 4744 (1986).
- [8] A. W. Sandvik, Stochastic method for analytic continuation of quantum monte carlo data, *Phys. Rev. B* **57**, 10287 (1998).
- [9] H. Shao, Y. Q. Qin, S. Capponi, S. Chesi, Z. Y. Meng, and A. W. Sandvik, Nearly deconfined spinon excitations in the square-lattice spin-1/2 heisenberg antiferromagnet, *Phys. Rev. X* **7**, 041072 (2017).
- [10] T. Li and F. Yang, Variational study of the neutron resonance mode in the cuprate superconductors, *Phys. Rev. B* **81**, 214509 (2010).
- [11] F. Ferrari, A. Parola, S. Sorella, and F. Becca, Dynamical structure factor of the  $J_1 - J_2$  heisenberg model in one dimension: The variational monte carlo approach, *Phys. Rev. B* **97**, 235103 (2018).
- [12] D. Hendry and A. E. Feiguin, Machine learning approach to dynamical properties of quantum many-body systems, *Phys. Rev. B* **100**, 245123 (2019).
- [13] U. Schollwöck, The density-matrix renormalization group in the age of matrix product states, *Annals of Physics* **326**, 96 (2011), january 2011 Special Issue.
- [14] K. A. Hallberg, Density-matrix algorithm for the calculation of dynamical properties of low-dimensional systems, *Phys. Rev. B* **52**, R9827 (1995).
- [15] P. E. Dargel, A. Honecker, R. Peters, R. M. Noack, and T. Pruschke, Adaptive lanczos-vector method for dynamic properties within the density matrix renormalization group, *Phys. Rev. B* **83**, 161104 (2011).
- [16] T. D. Kühner and S. R. White, Dynamical correlation functions using the density matrix renormalization group, *Phys. Rev. B* **60**, 335 (1999).
- [17] E. Jeckelmann, Dynamical density-matrix renormalization-group method, *Phys. Rev. B* **66**, 045114 (2002).
- [18] H. Benthien, F. Gebhard, and E. Jeckelmann, Spectral function of the one-dimensional hubbard model away from half filling, *Phys. Rev. Lett.* **92**, 256401 (2004).
- [19] A. Holzner, A. Weichselbaum, I. P. McCulloch, U. Schollwöck, and J. von Delft, Chebyshev matrix product state approach for spectral functions, *Phys. Rev. B* **83**, 195115 (2011).
- [20] F. A. Wolf, J. A. Justiniano, I. P. McCulloch, and U. Schollwöck, Spectral functions and time evolution from the chebyshev recursion, *Phys. Rev. B* **91**, 115144 (2015).
- [21] H. D. Xie, R. Z. Huang, X. J. Han, X. Yan, H. H. Zhao, Z. Y. Xie, H. J. Liao, and T. Xiang, Reorthonormalization of chebyshev matrix product states for dynamical correlation functions, *Phys. Rev. B* **97**, 075111 (2018).
- [22] S. R. White and A. E. Feiguin, Real-time evolution using the density matrix renormalization group, *Phys. Rev. Lett.* **93**, 076401 (2004).
- [23] A. J. Daley, C. Kollath, U. Schollwöck, and G. Vidal, Time-dependent density-matrix renormalization-group using adaptive effective hilbert spaces, *Journal of Statistical Mechanics: Theory and Experiment* **2004**, P04005 (2004).
- [24] J. Haegeman, J. I. Cirac, T. J. Osborne, I. Pizorn, H. Verschelde, and F. Verstraete, Time-dependent variational principle for quantum lattices, *Phys. Rev. Lett.* **107**, 070601 (2011).
- [25] M. P. Zaletel, R. S. K. Mong, C. Karrasch, J. E. Moore, and F. Pollmann, Time-evolving a matrix product state with long-ranged interactions, *Phys. Rev. B* **91**, 165112 (2015).
- [26] S. Paeckel, T. Köhler, A. Swoboda, S. R. Manmana, U. Schollwöck, and C. Hubig, Time-evolution methods for matrix-product states, *Annals of Physics* **411**, 167998 (2019).
- [27] S. R. White and I. Affleck, Spectral function for the  $s = 1$  heisenberg antiferromagnetic chain, *Phys. Rev. B* **77**, 134437 (2008).
- [28] R. G. Pereira, S. R. White, and I. Affleck, Exact edge singularities and dynamical correlations in spin-1/2 chains, *Phys. Rev. Lett.* **100**, 027206 (2008).
- [29] T. Barthel, U. Schollwöck, and S. R. White, Spectral functions in one-dimensional quantum systems at finite temperature using the density matrix renormalization group, *Phys. Rev. B* **79**, 245101 (2009).
- [30] Y. Tian and S. R. White, Matrix product state recursion methods for computing spectral functions of strongly correlated quantum systems, *Phys. Rev. B* **103**, 125142 (2021).
- [31] J. Haegeman, B. Pirvu, D. J. Weir, J. I. Cirac, T. J. Osborne, H. Verschelde, and F. Verstraete, Variational matrix product ansatz for dispersion relations, *Phys. Rev. B* **85**, 100408 (2012).
- [32] J. Haegeman, T. J. Osborne, and F. Verstraete, Post-matrix product state methods: To tangent space and beyond, *Phys. Rev. B* **88**, 075133 (2013).
- [33] J. Haegeman, S. Michalakis, B. Nachtergaele, T. J. Osborne, N. Schuch, and F. Verstraete, Elementary excitations in gapped quantum spin systems, *Phys. Rev. Lett.* **111**, 080401 (2013).
- [34] A. K. Bera, B. Lake, F. H. L. Essler, L. Vanderstraeten, C. Hubig, U. Schollwöck, A. T. M. N. Islam, A. Schneidewind, and D. L. Quintero-Castro, Spinon confinement in a quasi-one-dimensional anisotropic heisenberg mag-

- net, *Phys. Rev. B* **96**, 054423 (2017).
- [35] M. Van Damme, R. Vanhove, J. Haegeman, F. Verstraete, and L. Vanderstraeten, Efficient matrix product state methods for extracting spectral information on rings and cylinders, *Phys. Rev. B* **104**, 115142 (2021).
- [36] L. Vanderstraeten, J. Haegeman, T. J. Osborne, and F. Verstraete,  $s$  matrix from matrix product states, *Phys. Rev. Lett.* **112**, 257202 (2014).
- [37] L. Vanderstraeten, F. Verstraete, and J. Haegeman, Scattering particles in quantum spin chains, *Phys. Rev. B* **92**, 125136 (2015).
- [38] L. Vanderstraeten, J. Haegeman, F. Verstraete, and D. Poilblanc, Quasiparticle interactions in frustrated heisenberg chains, *Phys. Rev. B* **93**, 235108 (2016).
- [39] H. N. Phien, G. Vidal, and I. P. McCulloch, Infinite boundary conditions for matrix product state calculations, *Phys. Rev. B* **86**, 245107 (2012).
- [40] A. Milsted, J. Haegeman, T. J. Osborne, and F. Verstraete, Variational matrix product ansatz for nonuniform dynamics in the thermodynamic limit, *Phys. Rev. B* **88**, 155116 (2013).
- [41] V. Zauner, M. Ganahl, H. G. Evertz, and T. Nishino, Time evolution within a comoving window: scaling of signal fronts and magnetization plateaus after a local quench in quantum spin chains, *Journal of Physics: Condensed Matter* **27**, 425602 (2015).
- [42] J. Haegeman, C. Lubich, I. Oseledets, B. Vandereycken, and F. Verstraete, Unifying time evolution and optimization with matrix product states, *Phys. Rev. B* **94**, 165116 (2016).
- [43] H. F. Trotter, On the product of semi-groups of operators, *Proc. Amer. Math. Soc.* **10**, 545 (1959).
- [44] M. Suzuki, Generalized trotter's formula and systematic approximants of exponential operators and inner derivations with applications to many-body problems, *Comm. Math. Phys.* **51**, 183 (1976).
- [45] T. Barthel and Y. Zhang, Optimized Lie–Trotter–Suzuki decompositions for two and three non-commuting terms, *Annals of Physics* **418**, 168165 (2020).
- [46] B. Vanhecke, L. Vanderstraeten, and F. Verstraete, Symmetric cluster expansions with tensor networks, *Phys. Rev. A* **103**, L020402 (2021).
- [47] B. Vanhecke, D. Devoogdt, F. Verstraete, and L. Vanderstraeten, Simulating thermal density operators with cluster expansions and tensor networks, [arXiv:2112.01507](https://arxiv.org/abs/2112.01507) (2021).
- [48] L. Vanderstraeten, E. Wybo, N. Chepiga, F. Verstraete, and F. Mila, Spinon confinement and deconfinement in spin-1 chains, *Phys. Rev. B* **101**, 115138 (2020).
- [49] A. Imambekov, T. L. Schmidt, and L. I. Glazman, One-dimensional quantum liquids: Beyond the luttinger liquid paradigm, *Rev. Mod. Phys.* **84**, 1253 (2012).
- [50] B. Dalla Piazza, M. Mourigal, N. B. Christensen, G. Nilson, P. Tregenna-Piggott, T. Perring, M. Enderle, D. F. McMorrow, D. Ivanov, and H. M. Rønnow, Fractional excitations in the square-lattice quantum antiferromagnet, *Nature physics* **11**, 62 (2015).
- [51] R. Verresen, F. Pollmann, and R. Moessner, Quantum dynamics of the square-lattice heisenberg model, *Phys. Rev. B* **98**, 155102 (2018).
- [52] F. Ferrari and F. Becca, Spectral signatures of fractionalization in the frustrated heisenberg model on the square lattice, *Phys. Rev. B* **98**, 100405 (2018).
- [53] M. Powalski, K. P. Schmidt, and G. S. Uhrig, Mutually attracting spin waves in the square-lattice quantum antiferromagnet, *SciPost Phys.* **4**, 001 (2018).
- [54] W.-J. Hu, F. Becca, A. Parola, and S. Sorella, Direct evidence for a gapless  $Z_2$  spin liquid by frustrating néel antiferromagnetism, *Phys. Rev. B* **88**, 060402 (2013).
- [55] L. Vanderstraeten, J. Haegeman, and F. Verstraete, Simulating excitation spectra with projected entangled-pair states, *Phys. Rev. B* **99**, 165121 (2019).
- [56] M. Gohlke, R. Verresen, R. Moessner, and F. Pollmann, Dynamics of the kitaev-heisenberg model, *Phys. Rev. Lett.* **119**, 157203 (2017).
- [57] R. Verresen, R. Moessner, and F. Pollmann, Avoided quasiparticle decay from strong quantum interactions, *Nature Physics* **15**, 750 (2019).
- [58] C. Yang and A. E. Feiguin, Spectral function of mott-insulating hubbard ladders: From fractionalized excitations to coherent quasiparticles, *Phys. Rev. B* **99**, 235117 (2019).
- [59] A. Bohrdt, E. Demler, F. Pollmann, M. Knap, and F. Grusdt, Parton theory of angle-resolved photoemission spectroscopy spectra in antiferromagnetic mott insulators, *Phys. Rev. B* **102**, 035139 (2020).
- [60] L. Wang and H.-Q. Lin, Dynamic structure factor from real time evolution and exact correction vectors with matrix product states, [arXiv:1901.07751](https://arxiv.org/abs/1901.07751) (2019).
- [61] L. Vanderstraeten, M. Mariën, F. Verstraete, and J. Haegeman, Excitations and the tangent space of projected entangled-pair states, *Phys. Rev. B* **92**, 201111 (2015).
- [62] B. Ponsioen and P. Corboz, Excitations with projected entangled pair states using the corner transfer matrix method, *Phys. Rev. B* **101**, 195109 (2020).
- [63] L. Vanderstraeten, J. Haegeman, and F. Verstraete, Tangent-space methods for uniform matrix product states, *SciPost Physics Lecture Notes* , 007 (2019).
- [64] V. Zauner-Stauber, L. Vanderstraeten, J. Haegeman, I. P. McCulloch, and F. Verstraete, Topological nature of spinons and holons: Elementary excitations from matrix product states with conserved symmetries, *Phys. Rev. B* **97**, 235155 (2018).
- [65] L. Michel and I. P. McCulloch, Schur Forms of Matrix Product Operators in the Infinite Limit, [arXiv:1008.4667](https://arxiv.org/abs/1008.4667) (2010).
- [66] C. Hubig, I. P. McCulloch, and U. Schollwöck, Generic construction of efficient matrix product operators, *Phys. Rev. B* **95**, 035129 (2017).
- [67] D. E. Parker, X. Cao, and M. P. Zaletel, Local matrix product operators: Canonical form, compression, and control theory, *Phys. Rev. B* **102**, 035147 (2020).
- [68] J. C. Pillay and I. P. McCulloch, Cumulants and scaling functions of infinite matrix product states, *Phys. Rev. B* **100**, 235140 (2019).

## Appendix A: Momentum-window MPS

The class of momentum-window states on top of uniform MPS was introduced in Ref. 48, where it was used to simulate extended bound states of solitons in a spin-1 model. In this Appendix, we will explain the properties of this class of variational states in some detail, and indicate how to simulate time evolution.

**Properties**— We start from a uniform MPS (see Ref. 63 for details), which can be represented in center-site gauge as

$$|\Psi_0\rangle = \text{---} \begin{array}{c} | \\ \text{---} A_l \text{---} \\ | \end{array} \text{---} \begin{array}{c} | \\ \text{---} A_l \text{---} \\ | \end{array} \text{---} \begin{array}{c} | \\ \text{---} A_c \text{---} \\ | \end{array} \text{---} \begin{array}{c} | \\ \text{---} A_r \text{---} \\ | \end{array} \text{---} \begin{array}{c} | \\ \text{---} A_r \text{---} \\ | \end{array} \text{---}, \quad (\text{A1})$$

where  $A_l$  and  $A_r$  are left and right isometries. On top of this uniform MPS, a momentum-window state can be understood as the following state

$$\sum_n e^{iqn} \text{---} \begin{array}{c} | \\ \text{---} A_l \text{---} \\ | \end{array} \text{---} \begin{array}{c} | \\ \text{---} B \text{---} \\ | \end{array} \text{---} \begin{array}{c} | \\ \text{---} A_r \text{---} \\ | \end{array} \text{---}, \quad (\text{A2})$$

where  $n$  denotes the  $n$ 'th site in the chain. This class of states is a linear subspace in terms of the tensor  $B$ , and has residual gauge freedom since the following subclass of states

$$\sum_n e^{iqn} \left( \text{---} \begin{array}{c} | \\ \text{---} A_l \text{---} \\ | \end{array} \text{---} \begin{array}{c} | \\ \text{---} A_l \text{---} \\ | \end{array} \text{---} \begin{array}{c} | \\ \text{---} X \text{---} \\ | \end{array} \text{---} \begin{array}{c} | \\ \text{---} A_r \text{---} \\ | \end{array} \text{---} \right. \\ \left. - e^{iq} \text{---} \begin{array}{c} | \\ \text{---} A_l \text{---} \\ | \end{array} \text{---} \begin{array}{c} | \\ \text{---} X \text{---} \\ | \end{array} \text{---} \begin{array}{c} | \\ \text{---} A_r \text{---} \\ | \end{array} \text{---} \begin{array}{c} | \\ \text{---} A_r \text{---} \\ | \end{array} \text{---} \right) \quad (\text{A3})$$

yields a zero norm. If we assume that the window state is orthogonal to the ground-state MPS, then we can absorb this gauge freedom entirely by constraining  $B$  to be of the form

$$\text{---} \begin{array}{c} | \\ \text{---} B \text{---} \\ | \end{array} \text{---} = \text{---} \begin{array}{c} | \\ \text{---} V_l \text{---} \\ | \end{array} \text{---} \begin{array}{c} | \\ \text{---} X \text{---} \\ | \end{array} \text{---}, \quad (\text{A4})$$

with  $V_l$  being the null space of  $A_l$ , satisfying

$$\begin{array}{c} | \\ \text{---} V_l \text{---} \\ | \end{array} \begin{array}{c} | \\ \text{---} A_l \text{---} \\ | \end{array} = 0, \quad \begin{array}{c} | \\ \text{---} V_l \text{---} \\ | \end{array} \begin{array}{c} | \\ \text{---} V_l \text{---} \\ | \end{array} = \left( \cdot \right). \quad (\text{A5})$$

Working with such an extended block tensor the variational parameters scale exponentially with the size of the block, so we make the approximation of decomposing  $X$  as a finite MPS

$$\text{---} \begin{array}{c} | \\ \text{---} B \text{---} \\ | \end{array} \text{---} = \text{---} \begin{array}{c} | \\ \text{---} V_l \text{---} \\ | \end{array} \text{---} \begin{array}{c} | \\ \text{---} X_1 \text{---} \\ | \end{array} \text{---} \begin{array}{c} | \\ \text{---} X_2 \text{---} \\ | \end{array} \text{---}, \quad (\text{A6})$$

so that we arrive at our variational class of momentum-window MPS or “ $q$ -MPS” as

$$|\Phi_q(X)\rangle = \sum_n e^{iqn} \text{---} \begin{array}{c} | \\ \text{---} A_l \text{---} \\ | \end{array} \text{---} \begin{array}{c} | \\ \text{---} V_l \text{---} \\ | \end{array} \text{---} \begin{array}{c} | \\ \text{---} X_1 \text{---} \\ | \end{array} \text{---} \begin{array}{c} | \\ \text{---} X_2 \text{---} \\ | \end{array} \text{---} \begin{array}{c} | \\ \text{---} A_r \text{---} \\ | \end{array} \text{---}. \quad (\text{A7})$$

This class of  $q$ -MPS can be utilized in much the same way as a “usual” finite MPS. After all, the overlap of two

different  $q$ -MPSs simplifies to the overlap between their respective windows:

$$\langle \Phi_q(X) | \Phi_{q'}(X') \rangle = 2\pi\delta(q - q') \langle \Phi_q(X) | \Phi_q(X') \rangle_{\text{finite}} \quad (\text{A8})$$

with

$$\langle \Phi_q(X) | \Phi_q(X') \rangle_{\text{finite}} = \begin{array}{c} \begin{array}{c} | \\ \text{---} X'_1 \text{---} \\ | \end{array} \text{---} \begin{array}{c} | \\ \text{---} X'_2 \text{---} \\ | \end{array} \text{---} \dots \text{---} \begin{array}{c} | \\ \text{---} X'_N \text{---} \\ | \end{array} \\ \begin{array}{c} | \\ \text{---} X_1 \text{---} \\ | \end{array} \text{---} \begin{array}{c} | \\ \text{---} X_2 \text{---} \\ | \end{array} \text{---} \dots \text{---} \begin{array}{c} | \\ \text{---} X_N \text{---} \\ | \end{array} \end{array}. \quad (\text{A9})$$

This means that the orthogonality center can be shifted through the window by consecutive orthogonal matrix decompositions, and we can therefore directly translate most algorithms from their real-space to the momentum-space setting!

**Energy minimization**— As a first example, we can consider a direct energy minimization by sweeping through the window, similarly as the standard DMRG algorithm for ground states of a finite spin chain [13]. Indeed, we can iteratively solve eigenvalue problems, pushing the orthogonality center at site  $n$  around:

$$(H_{\text{eff}})_{nn} X_n = \lambda X_n. \quad (\text{A10})$$

Because our ansatz has a well defined momentum and is by construction orthogonal to the ground state, we will be directly targeting the lowest-lying excitations. This algorithm was used in Ref. 48 for simulating dispersion relations of broad bound states in a spin chain.

The calculation of  $H_{\text{eff}}$  is quite straightforward, it is defined as

$$(H_{\text{eff}})_{ij} = \frac{\partial^2}{\partial X_i \partial X_j} \langle \Phi_q(X) | H | \Phi_q(X) \rangle_{\text{finite}}, \quad (\text{A11})$$

where we are typically only interested in the diagonal entries: when sweeping through the window we only vary one tensor, see Eq.(A10).

Here, the energy expectation value is the momentum sum of all possible different positions of a window in the top and bottom layer. For two normalized  $q$ -MPS parametrized by  $X$  and  $X'$  and the Hamiltonian represented as a matrix product operator (MPO) [13], we would require the following sums:

$$\langle \Phi_q(X) | H | \Phi_q(X) \rangle_{\text{finite}} = \sum_{n' > n} e^{i(n-n')q} \begin{array}{c} \begin{array}{c} | \\ \text{---} B_n(X_1, X_2) \text{---} \\ | \end{array} \text{---} \begin{array}{c} | \\ \text{---} A_r \text{---} \\ | \end{array} \text{---} \begin{array}{c} | \\ \text{---} A_r \text{---} \\ | \end{array} \text{---} \begin{array}{c} | \\ \text{---} A_r \text{---} \\ | \end{array} \text{---} \\ \begin{array}{c} | \\ \text{---} O \text{---} \\ | \end{array} \text{---} \begin{array}{c} | \\ \text{---} O \text{---} \\ | \end{array} \text{---} \begin{array}{c} | \\ \text{---} O \text{---} \\ | \end{array} \text{---} \dots \text{---} \begin{array}{c} | \\ \text{---} O \text{---} \\ | \end{array} \text{---} \begin{array}{c} | \\ \text{---} O \text{---} \\ | \end{array} \text{---} \begin{array}{c} | \\ \text{---} O \text{---} \\ | \end{array} \text{---} \rho_r \\ \begin{array}{c} | \\ \text{---} A_l \text{---} \\ | \end{array} \text{---} \begin{array}{c} | \\ \text{---} A_l \text{---} \\ | \end{array} \text{---} \begin{array}{c} | \\ \text{---} A_l \text{---} \\ | \end{array} \text{---} \\ \begin{array}{c} | \\ \text{---} B_{n'}(X'_1, X'_2) \text{---} \\ | \end{array} \end{array} \\ + \sum_{n' < n} e^{i(n-n')q} \begin{array}{c} \begin{array}{c} | \\ \text{---} A_l \text{---} \\ | \end{array} \text{---} \begin{array}{c} | \\ \text{---} A_l \text{---} \\ | \end{array} \text{---} \begin{array}{c} | \\ \text{---} A_l \text{---} \\ | \end{array} \text{---} \\ \begin{array}{c} | \\ \text{---} O \text{---} \\ | \end{array} \text{---} \begin{array}{c} | \\ \text{---} O \text{---} \\ | \end{array} \text{---} \begin{array}{c} | \\ \text{---} O \text{---} \\ | \end{array} \text{---} \dots \text{---} \begin{array}{c} | \\ \text{---} O \text{---} \\ | \end{array} \text{---} \begin{array}{c} | \\ \text{---} O \text{---} \\ | \end{array} \text{---} \begin{array}{c} | \\ \text{---} O \text{---} \\ | \end{array} \text{---} \rho_r \\ \begin{array}{c} | \\ \text{---} B_{n'}(X'_1, X'_2) \text{---} \\ | \end{array} \end{array} \\ + e^{iq} \begin{array}{c} \begin{array}{c} | \\ \text{---} A_l \text{---} \\ | \end{array} \text{---} \begin{array}{c} | \\ \text{---} B_{n'+1}(X_1, X_2) \text{---} \\ | \end{array} \text{---} \\ \begin{array}{c} | \\ \text{---} O \text{---} \\ | \end{array} \text{---} \begin{array}{c} | \\ \text{---} O \text{---} \\ | \end{array} \text{---} \begin{array}{c} | \\ \text{---} O \text{---} \\ | \end{array} \text{---} \begin{array}{c} | \\ \text{---} O \text{---} \\ | \end{array} \text{---} \rho_r \\ \begin{array}{c} | \\ \text{---} B_{n'}(X'_1, X'_2) \text{---} \\ | \end{array} \end{array} \end{array}$$

$$\begin{aligned}
& + e^{i2q} \left[ \begin{array}{c} \rho_l \text{---} [A_l \text{---} A_l \text{---} B_{n'+2}(X_1, X_2)] \text{---} \rho_r \\ | \quad | \quad | \quad | \quad | \\ \text{---} O \text{---} O \text{---} O \text{---} O \text{---} O \text{---} \\ | \quad | \quad | \quad | \\ \text{---} B_{n'}(X'_1, X'_2) \text{---} A_r \text{---} A_r \end{array} \right] \\
& + e^{-iq} \left[ \begin{array}{c} \rho_l \text{---} [B_{n'-1}(X_1, X_2) \text{---} A_r] \text{---} \rho_r \\ | \quad | \quad | \quad | \\ \text{---} O \text{---} O \text{---} O \text{---} O \text{---} \\ | \quad | \quad | \\ \text{---} A_l \text{---} B_{n'}(X'_1, X'_2) \end{array} \right] \\
& + e^{-i2q} \left[ \begin{array}{c} \rho_l \text{---} [B_{n'-2}(X_1, X_2) \text{---} A_r \text{---} A_r] \text{---} \rho_r \\ | \quad | \quad | \quad | \quad | \\ \text{---} O \text{---} O \text{---} O \text{---} O \text{---} O \text{---} \\ | \quad | \quad | \quad | \\ \text{---} A_l \text{---} A_l \text{---} B_{n'}(X'_1, X'_2) \end{array} \right] \\
& + \left[ \begin{array}{c} \rho_l \text{---} [B_{n'}(X_1, X_2)] \text{---} \rho_r \\ | \quad | \quad | \\ \text{---} O \text{---} O \text{---} O \text{---} \\ | \quad | \quad | \\ \text{---} B_{n'}(X'_1, X'_2) \end{array} \right]. \tag{A12}
\end{aligned}$$

Here, the first two sums are over  $n$ , whereas the index  $n'$  is an arbitrary site in the lattice; the prescription  $\langle \dots \rangle_{\text{finite}}$  denotes that we have taken out one infinite sum that occurs when taking overlaps of momentum states, see Eq. (A8). The first two sums contain an infinite amount of terms, and can be summed by solving the linear problem:

$$\left[ \begin{array}{c} \rho_l \text{---} [B(X_1, X_2)] \text{---} \\ | \quad | \quad | \\ \text{---} O \text{---} O \text{---} O \text{---} \\ | \quad | \quad | \\ \text{---} A_l \text{---} A_l \text{---} A_l \end{array} \right] \left( 1 - e^{-iq} \begin{array}{c} -A_r \\ -O \\ -A_l \end{array} \right)^{-1}. \tag{A13}$$

This type of infinite summation always occurs when working with momentum states on top of uniform MPS, and details can be found in Ref. 63. This linear problem has to be recomputed every time that any  $X_n$  changes, which makes some sweeping algorithms more expensive compared to their finite MPS counterparts. Importantly, however, if a tensor in the bra changes we do not have to recompute these contributions!

**Initial state**— In the main text we have looked at real-time evolution within the class of momentum-window MPS, where the initial state is a momentum operator on the ground state. The initial state is of the form

$$\sum_n e^{iqn} O_n |\Psi_0\rangle = \text{---} [A_l \text{---} O \text{---} A_r] \text{---}_n, \tag{A14}$$

which can be brought under the form of Eq. A7 by maximizing the overlap with a two-site window. Since this optimization problem is linear in  $X_1$ , the solution is simply

$$X_1 = \frac{\partial}{\partial X_1} \langle \Phi_q(X_1) | \sum_n e^{iqn} O_n |\Psi_0\rangle \tag{A15}$$

The overlap in question is given by the terms

$$\begin{aligned}
& \left[ \begin{array}{c} O \text{---} A_r \\ | \quad | \\ \text{---} V_l \text{---} X_1 \end{array} \right] + e^{-iq} \left[ \begin{array}{c} O \text{---} A_r \text{---} A_r \\ | \quad | \quad | \\ \text{---} A_r \text{---} V_l \text{---} X_1 \end{array} \right] \\
& + e^{-2iq} \left[ \begin{array}{c} O \text{---} A_r \text{---} A_r \text{---} A_r \\ | \quad | \quad | \quad | \\ \text{---} A_l \text{---} A_l \text{---} V_l \text{---} X_1 \end{array} \right] + \dots, \tag{A16}
\end{aligned}$$

where the latter terms can be summed as

$$e^{-iq} \left[ \begin{array}{c} O \\ | \\ A_l \end{array} \right] \left( 1 - e^{-iq} \begin{array}{c} -A_r \\ -A_l \end{array} \right)^{-1} \left[ \begin{array}{c} -A_r \text{---} A_r \\ | \quad | \\ -V_l \text{---} X_1 \end{array} \right]. \tag{A17}$$

Again, this type of infinite summation is usual when working with momentum states on top of uniform MPS [63].

After having reformulated the initial state as a  $q$ -MPS, we can perform the actual time evolution. Here, we can choose between applying the time-dependent variational principle (TDVP) [24, 42] or applying an MPO representation for the time-evolution operator with variational truncation.

**TDVP**— For applying the TDVP, we require the same  $H_{\text{eff}}$  as in  $q$ -MPS energy minimization. The resulting algorithm is identical to the well known finite-MPS variant as in Ref. 42, where for every time step  $\delta t$  one sweeps through the tensors and evolves the tensors as: (i) evolve the current orthogonality center as

$$e^{-\frac{i\delta t}{2} H_{\text{eff}}}(X_i) = X'_i, \tag{A18}$$

(ii) using QR or RQ decompositions we can then left- or right-orthogonalize  $X'_i$ , (iii) subsequently evolve the resulting  $R$  backwards in time,

$$e^{-\frac{i\delta t}{2} H_{\text{eff}}}(R) = R', \tag{A19}$$

and (iv) absorb  $R'$  in the next tensor. Note that the exponentials can be implemented iteratively such that only the action of  $H_{\text{eff}}$  is needed on a given tensor; the action of  $H_{\text{eff}}$  on the tensor  $X_i$  is the same as the one in Eq. (A10), whereas the action on a link matrix  $R$  can be found by projecting the same  $H_{\text{eff}}$  [42]. After a full forward and backwards sweep, we have evolved the entire window forward with one time step  $\delta t$ .

We note that this algorithm is rather expensive, as every exponentiation step has to be done iteratively and  $H_{\text{eff}}(X)$  can re-use very little information between applications on the different  $X_i$  in the window. This is in contrast to the usual finite-MPS setting where  $H_{\text{eff}}(X)$  can be updated by a single contraction to the next site in the chain.

**MPO time evolution**— Applying an MPO to a  $q$ -MPS goes as follows. In each time step, we want to update the  $X$  tensors as

$$|\Phi_q(X')\rangle \approx U(\delta t) |\Phi_q(X)\rangle, \tag{A20}$$

where the  $\approx$  sign can be interpreted variationally as minimizing the norm between these two states. Solving this minimization problem can be done, again, by a sweeping algorithm, where we sweep over the  $X'$  tensors until convergence. By shifting the orthogonality center accordingly, the minimization problem for a single  $X'$  tensor is simply solved as

$$X'_i = \frac{\partial}{\partial X'_i} \langle \Phi_q(X') | U(\delta t) |\Phi_q(X)\rangle_{\text{finite}}. \tag{A21}$$

This quantity is a sum of different terms: Because the MPO is between bra and ket layer, one does not have the nice property that only one term survives as in Eq. (A8). The term where the two windows are located on the same region is proportional to

$$\left[ \begin{array}{c} \text{---} \\ | \\ G_l \\ | \\ \text{---} \\ V_l \\ | \\ U \\ | \\ \text{---} \\ X_1 \\ | \\ X_2 \\ | \\ X_3 \\ | \\ \text{---} \\ V_l \\ | \\ U \\ | \\ \text{---} \\ X_1' \\ | \\ X_2' \\ | \\ X_3' \\ | \\ \text{---} \\ G_r \\ | \\ \text{---} \end{array} \right], \quad (\text{A22})$$

where the  $U$  tensor encodes the MPO representation of the time-evolution operator (see App. B), and with  $G_l$  the fixed point of the channel

$$\left[ \begin{array}{c} \text{---} \\ | \\ G_l \\ | \\ \text{---} \\ A_l \\ | \\ U \\ | \\ \text{---} \\ A_l \\ | \\ \text{---} \end{array} \right] = \lambda \left[ \begin{array}{c} \text{---} \\ | \\ G_l \\ | \\ \text{---} \end{array} \right], \quad (\text{A23})$$

and a similar equation for  $G_r$ . If the uniform MPS is close to the ground state and  $U(\delta)$  is close to an exact representation of  $e^{-i(H-E_0)\delta t}$ , then the eigenvalue  $\lambda$  is close to one. It is convenient to explicitly rescale the MPO tensor for  $U(\delta t)$  such that this eigenvalue is exactly equal to one. We also require the fixed points to be normalized as

$$\left[ \begin{array}{c} \text{---} \\ | \\ G_l \\ | \\ \text{---} \\ A_c \\ | \\ U \\ | \\ \text{---} \\ A_c \\ | \\ \text{---} \\ G_r \\ | \\ \text{---} \end{array} \right] = 1. \quad (\text{A24})$$

Then the above diagram in Eq. (A22) also appears as a term without a prefactor.

Other terms are of the form

$$\left[ \begin{array}{c} \text{---} \\ | \\ G_l \\ | \\ \text{---} \\ A_l \\ | \\ U \\ | \\ \text{---} \\ A_l \\ | \\ \text{---} \\ V_l \\ | \\ X_1 \\ | \\ X_2 \\ | \\ X_3 \\ | \\ \text{---} \\ V_l \\ | \\ X_1' \\ | \\ X_2' \\ | \\ X_3' \\ | \\ \text{---} \\ A_r \\ | \\ A_r \\ | \\ \text{---} \\ G_r \\ | \\ \text{---} \end{array} \right], \quad (\text{A25})$$

and should all be summed. The infinite number of disconnected terms can be explicitly summed by solving a linear problem:

$$\left[ \begin{array}{c} \text{---} \\ | \\ G_l \\ | \\ \text{---} \\ A_l \\ | \\ U \\ | \\ \text{---} \\ V_l \\ | \\ X_1' \\ | \\ X_2' \\ | \\ X_3' \\ | \\ \text{---} \end{array} \right] \left( 1 - e^{-iq} \begin{array}{c} \text{---} \\ | \\ A_l \\ | \\ U \\ | \\ \text{---} \\ A_r \\ | \\ \text{---} \end{array} \right)^{-1} \left[ \begin{array}{c} \text{---} \\ | \\ V_l \\ | \\ X_1 \\ | \\ X_2 \\ | \\ X_3 \\ | \\ \text{---} \\ U \\ | \\ U \\ | \\ U \\ | \\ \text{---} \\ A_r \\ | \\ A_r \\ | \\ \text{---} \\ G_r \\ | \\ \text{---} \end{array} \right], \quad (\text{A26})$$

as is usual for working with momentum states on uniform MPS, see Ref. 63 for details. Summing up all these terms allows us to compute the expression in Eq. (A21) and to update the tensor  $X_i'$ .

Note that in the course of sweeping through the window, the different contributions to Eq. (A21) do not need to be computed from scratch, but the environments can be updated by a single contraction. This is very similar to a real-space window optimization, only are there

a number of different terms to take into account. These updates can be performed in parallel, so with enough parallel workers the optimization in each time step does not need to take more time than the real-space approach. Given that we can reduce the bond dimension significantly in momentum space (as shown in the main text), the momentum-space approach is more efficient for obtaining a single momentum cut of the spectral function.

**Larger unit cells**— Until now we have explained everything for uniform MPS with a single-site unit cell, but larger unit cells often need to be considered, particularly if we consider multi-leg ladders or cylindrical geometries. The extension to larger unit cells is mainly a matter of more intricate bookkeeping, but it is useful to write down the expressions for a  $q$ -MPS. We will describe the case of two-site unit cells, larger unit cells follow trivially.

A two-site uniform MPS is given by

$$|\Psi_0\rangle = \text{---} \left[ \begin{array}{c} \text{---} \\ | \\ A_l^1 \\ | \\ \text{---} \\ A_l^2 \\ | \\ \text{---} \\ A_c^1 \\ | \\ \text{---} \\ A_c^2 \\ | \\ \text{---} \\ A_r^1 \\ | \\ \text{---} \\ A_r^2 \\ | \\ \text{---} \end{array} \right] \text{---} \quad (\text{A27})$$

$$= \text{---} \left[ \begin{array}{c} \text{---} \\ | \\ A_l^1 \\ | \\ \text{---} \\ A_l^2 \\ | \\ \text{---} \\ A_c^1 \\ | \\ \text{---} \\ A_c^2 \\ | \\ \text{---} \\ A_r^1 \\ | \\ \text{---} \\ A_r^2 \\ | \\ \text{---} \end{array} \right] \text{---}. \quad (\text{A28})$$

As explained in Ref. 64, a momentum state on top of such an MPS is given by

$$\sum_{n \in 2\mathbb{Z}} e^{iqn} \left( \text{---} \left[ \begin{array}{c} \text{---} \\ | \\ A_l^1 \\ | \\ \text{---} \\ A_l^2 \\ | \\ \text{---} \\ B_n^1 \\ | \\ \text{---} \\ B_n^2 \\ | \\ \text{---} \\ A_r^1 \\ | \\ \text{---} \\ A_r^2 \\ | \\ \text{---} \end{array} \right] \text{---} + \text{---} \left[ \begin{array}{c} \text{---} \\ | \\ A_l^1 \\ | \\ \text{---} \\ A_l^2 \\ | \\ \text{---} \\ A_l^1 \\ | \\ \text{---} \\ B_n^2 \\ | \\ \text{---} \\ B_n^1 \\ | \\ \text{---} \\ A_r^1 \\ | \\ \text{---} \\ A_r^2 \\ | \\ \text{---} \end{array} \right] \text{---} \right), \quad (\text{A29})$$

i.e. we take two different  $B$  tensors for each of two sites within the unit cell. The extension of this to a momentum-window state is of the form

$$|\Phi_q(X^1, X^2)\rangle = \sum_{n \in 2\mathbb{Z}} e^{iqn} \left( \text{---} \left[ \begin{array}{c} \text{---} \\ | \\ A_l^1 \\ | \\ \text{---} \\ A_l^2 \\ | \\ \text{---} \\ V_n^1 \\ | \\ \text{---} \\ V_n^2 \\ | \\ \text{---} \\ X_1^1 \\ | \\ X_2^1 \\ | \\ X_3^1 \\ | \\ \text{---} \\ X_1^2 \\ | \\ X_2^2 \\ | \\ X_3^2 \\ | \\ \text{---} \\ A_r^1 \\ | \\ \text{---} \\ A_r^2 \\ | \\ \text{---} \end{array} \right] \text{---} + \text{---} \left[ \begin{array}{c} \text{---} \\ | \\ A_l^1 \\ | \\ \text{---} \\ A_l^2 \\ | \\ \text{---} \\ A_l^1 \\ | \\ \text{---} \\ V_n^2 \\ | \\ \text{---} \\ V_n^1 \\ | \\ \text{---} \\ X_1^2 \\ | \\ X_2^2 \\ | \\ X_3^2 \\ | \\ \text{---} \\ X_1^1 \\ | \\ X_2^1 \\ | \\ X_3^1 \\ | \\ \text{---} \\ A_r^1 \\ | \\ \text{---} \\ A_r^2 \\ | \\ \text{---} \end{array} \right] \text{---} \right). \quad (\text{A30})$$

Note that an alternative choice would consist of taking a single window that represents the sum of the two windows, but this would require a larger bond dimension. In particular, a momentum operator can be represented using the above expression without changing the bond dimension, whereas representing this with a single window would require us to double the bond dimension within the window.

The definition of the  $q$ -MPS with inclusion of the null-space projectors  $V_l^i$  makes sure that the inner product remains of a simple euclidean form

$$\langle \Phi_{q'}(X'^1, X'^2) | \Phi_q(X^1, X^2) \rangle_{\text{finite}} = \sum_i \left( \begin{array}{c} \text{---} \\ | \\ X_1^1 \\ | \\ \text{---} \\ X_2^1 \\ | \\ \text{---} \\ X_3^1 \\ | \\ \text{---} \\ X_1^2 \\ | \\ \text{---} \\ X_2^2 \\ | \\ \text{---} \\ X_3^2 \\ | \\ \text{---} \end{array} \right). \quad (\text{A31})$$

Therefore, a sweeping algorithm can still be used for energy minimization and MPO time evolution. For the former, the effective hamiltonian does not diagonalize in the different windows and cross terms need to be taken into account. For the MPO time-evolution, however, the sweeping procedure over the tensors in each window is completely independent from the others, so we can parallelize these completely!

### Appendix B: Time-evolution MPOs

In this Appendix we show how one can systematically construct an MPO representation of the time-evolution operator accurate up to  $n$ 'th order. We will demonstrate the algorithm by deriving the second-order time evolution MPO, and end with pseudo-code for the more general  $n$ 'th order algorithm.

We start from the MPO representation of a generic spin-chain Hamiltonian  $H$  [13, 65, 66],

$$H = \begin{pmatrix} \hat{\mathbb{I}} & \hat{C} & \hat{D} \\ & \hat{A} & \hat{B} \\ & & \hat{\mathbb{I}} \end{pmatrix}. \quad (\text{B1})$$

This operator is a ‘‘first-degree’’ MPO [67], in the sense that it cannot be normalized to a finite value in the thermodynamic limit but that the norm scales linearly with

system size – as it should for a local operator. This is reflected in the fact that the above form contains a single Jordan block, and it is required that the diagonal  $\hat{A}$  part has spectral radius smaller than one. In Ref. 25 it was shown that a simple MPO of the form

$$W_1(\tau) = \begin{pmatrix} \hat{\mathbb{I}} + \tau \hat{D} & \tau \hat{C} \\ \hat{B} & \hat{A} \end{pmatrix} \quad (\text{B2})$$

serves as a first-order approximation of the time evolution operator  $e^{H\tau}$ . As explained in Ref. 25, this operator is extensive and contains all higher-order terms in the expansion in which different actions of the Hamiltonian do not overlap. The cluster expansion [46, 47] can be seen as a systematic improvement on this MPO, such that overlapping contributions (i.e., clusters) are also included, but this works for strictly local Hamiltonians only. For general Hamiltonians of the above form, we can go to higher orders in the following way.

We start by rewriting the Hamiltonian in table form:

$$H \sim \begin{array}{|c|c|c|c|} \hline & 1 & 2 & 3 \\ \hline 1 & \mathbb{I} & C & D \\ \hline 2 & & A & B \\ \hline 3 & & & \mathbb{I} \\ \hline \end{array}, \quad (\text{B3})$$

where we have omitted hats on the operators.

We can now represent the product of this Hamiltonian with itself as a sparse MPO of the form

$$H^2 \sim \begin{array}{|c|c|c|c|c|c|c|c|c|c|} \hline & (1,1) & (1,2) & (1,3) & (2,1) & (2,2) & (2,3) & (3,1) & (3,2) & (3,3) \\ \hline (1,1) & \mathbb{I} & C & D & C & CC & CD & D & DC & DD \\ \hline (1,2) & & A & B & & CA & CB & & DA & DB \\ \hline (1,3) & & & \mathbb{I} & & & C & & & D \\ \hline (2,1) & & & & A & AC & AD & B & BC & BD \\ \hline (2,2) & & & & & AA & AB & & BA & BB \\ \hline (2,3) & & & & & & A & & & B \\ \hline (3,1) & & & & & & & \mathbb{I} & C & D \\ \hline (3,2) & & & & & & & & A & D \\ \hline (3,3) & & & & & & & & & \mathbb{I} \\ \hline \end{array}. \quad (\text{B4})$$

This form has two Jordan blocks representing a second-degree MPO and can be evaluated using the methods of Refs. 65 and 68. Taking the exponential version of this operator, similarly as we did for getting from  $H$  to the  $W_1(\tau)$  operator, now requires a few steps. The first step is to take the column (1,3), multiply by  $\tau$ , and add to the first column. The second step is to take the (3,3) column, multiply by  $\frac{\tau^2}{2}$ , and add to the first column. In the last step, we remove the rows and columns (1,3), (3,1) and (3,3):

$$W_2(\tau) \sim \begin{array}{|c|c|c|c|c|c|c|} \hline & (1,1) & (1,2) & (2,1) & (2,2) & (2,3) & (3,2) \\ \hline (1,1) & \mathbb{I} + \tau D + \tau^2/2 DD & C & C & CC & CD & DC \\ \hline (1,2) & \tau B + \tau^2/2 DB & A & & CA & CB & DA \\ \hline (2,1) & \tau^2/2 BD & & A & AC & AD & BC \\ \hline (2,2) & \tau^2/2 BB & & & AA & AB & BA \\ \hline (2,3) & \tau^2/2 B & & & & A & \\ \hline (3,2) & \tau^2/2 D & & & & & A \\ \hline \end{array}, \quad (\text{B5})$$

and all other components are zero.

This procedure is straightforward to generalize. Assuming an MPO representation of a Hamiltonian with bond dimension  $D$ , and wanting the correct time-evolution operator up to order  $N$  we would:

- multiply the Hamiltonian  $N$  times with itself
  - add  $\tau$  times the  $(1, 1, \dots, 1, 1, 1, D)$  column to the first column
  - add  $\tau^2/2$  times the  $(1, 1, \dots, 1, 1, D, D)$  column to the first column
  - ...
  - add  $\tau^N/N!$  times the  $(D, D, \dots, D, D, D, D)$  column to the first column

- 
- remove all columns and rows with label only containing 1 or  $D$ , except  $(1, 1, \dots, 1)$ .

This  $N$ -th order MPO has a bond dimension of  $D^N - 2^N + 1$ , with a worst case of approximately 1/2 sparseness. For a nearest-neighbour Hamiltonian with on-site interactions there is no  $C$  block, and the resulting MPO is much sparser. As an example, the third-order MPO for the Ising Hamiltonian has a bond dimension 20, but only 63 of the 400 blocks are non-zero.